Shantanu Mishra, Doreen Beyer, Reinhard Berger, Junzhi Liu, Oliver Gröning, José I. Urgel, Klaus Müllen, Pascal Ruffieux, Xinliang Feng, Roman Fasel

# Topological Defect-Induced Magnetism in a Nanographene

**Erstveröffentlichung in / First published in:**

*Journal of the American Chemical Society*. 2019, 142 (3), S. 1147–1152. ACS Publications. ISSN 1520-5126

DOI: https://doi.org/10.1021/jacs.9b09212

Final edited form was published in "Journal of the American Chemical Society". 2019, 142 (3), S. 1147–1152. ISSN 1520-5126
https://doi.org/10.1021/jacs.9b09212

# Topological defect-induced magnetism in a nanographene

Shantanu Mishra[†], Doreen Beyer[§], Reinhard Berger[§], Junzhi Liu[§], Oliver Gröning[†], José I. Urgel[†], Klaus Müllen[¶], Pascal Ruffieux[†], Xinliang Feng[§,*] and Roman Fasel[†,‡,*]

[†]nanotech@surfaces Laboratory, Empa − Swiss Federal Laboratories for Materials Science and Technology, Dübendorf, Switzerland

[§]Faculty of Chemistry and Food Chemistry, and Center for Advancing Electronics Dresden, Technical University of Dresden, Dresden, Germany

[¶]Department of Synthetic Chemistry, Max Planck Institute for Polymer Research, Mainz, Germany

[‡]Department of Chemistry and Biochemistry, University of Bern, Bern, Switzerland

**ABSTRACT:** The on-surface reactions of 10-bromo-10'-(2,6-dimethylphenyl)-9,9'-bianthracene on Au(111) surface have been investigated by a combination of bond-resolved scanning tunneling microscopy, scanning tunneling spectroscopy, and tight-binding and mean-field Hubbard calculations. The reactions afford the synthesis of two open-shell nanographenes (**1a** and **1b**) exhibiting different scenarios of all-carbon magnetism. **1a**, an all-benzenoid nanographene with previously unreported triangulene-like termini, contains a high proportion of zigzag edges, which endows it with an exceedingly low frontier gap of 110 meV and edge-localized states. The dominant reaction product (**1b**) is a non-benzenoid nanographene consisting of a single pentagonal ring in a benzenoid framework. The presence of this non-benzenoid topological defect, which alters the bond connectivity in the hexagonal lattice, results in a non-Kekulé nanographene with a spin $S = ½$, which is detected as a Kondo resonance. Our work provides evidence of all-carbon magnetism, and motivates the use of topological defects as structural elements toward engineering magnetism in carbon-based nanomaterials for spintronics.

Inducing magnetism in carbon nanomaterials has been a long-standing challenge encompassing organic chemistry, materials science and condensed matter physics.[1] Owing to lower spin-orbit and hyperfine couplings,[1,2] and larger spin correlation lengths,[3] carbon nanomaterials are postulated to exhibit improved performance over current d- or f-block elements in high fidelity spin-based information processing.[1,4,5] The field of carbon magnetism has received a revived interest since developments in the bottom-up synthetic chemistry of polycyclic conjugated hydrocarbons, or nanographenes (NGs).[6] The electronic structure of NGs exhibits sensitive dependence on the topology of the π-electron network, which provides for a convenient platform to rationally engineer a plethora of properties, including magnetism. The radical nature of magnetic, open-shell NGs makes a conventional solution-based synthesis difficult, and in this regard, on-surface synthesis[7] under ultrahigh vacuum conditions has emerged as a powerful synthetic toolbox to realize highly reactive compounds. Current progress in the synthesis of open-shell NGs is largely limited to low-spin NGs with extended zigzag edges[8–20] or high-spin non-Kekulé NGs with sublattice imbalance.[21–27] However, much less attention has been paid on the potential of topological defects, in particular non-benzenoid rings, in inducing magnetism in NGs. Non-benzenoid rings, routinely observed as defects in graphene,[28] may significantly influence the chemical[29] and electronic[15,30–32] properties as a result of local changes in strain and conjugation. Here, we report a combined in-solution and on-surface synthesis of two open-shell NGs resulting from on-surface reactions of a single molecular precursor 10-bromo-10'-(2,6-dimethylphenyl)-9,9'-bianthracene (**2**, Scheme 1) on Au(111) surface, and their detailed study using scanning tunneling microscopy (STM) and spectroscopy (STS), supported by tight-binding (TB) and mean-field Hubbard (MFH) calculations. Surface-catalyzed Ullmann coupling and subsequent cyclodehydrogenation and oxidative cyclization reactions of **2** leads to the formation of two distinct NGs. **1a**, an all-benzenoid NG formed in minority, results from a defect-free on-surface reaction of **2** and consists of triangulene-like termini which present hitherto unreported extended zigzag edges exhibiting localized edge states with an antiferromagnetic coupling, and an exceedingly low frontier gap of 110 meV. Interestingly, we observe that a majority of Ullmann-coupled dimers of **2** lose a single methyl group, leading to the formation of a pentagonal ring in an otherwise all-benzenoid framework (**1b**). The presence of this topological defect renders **1b** a non-Kekulé NG with a single unpaired electron, which manifests as a Kondo resonance.[33]

The solution synthesis of **2** (Scheme 1) commenced with the formation of 9,9'-bianthracene (**4**), derived from commercially available 9,10-anthraquinone (**3**). The synthesis was carried out according to literature protocol,[34] and **4** was isolated as a yellow solid in moderate yield. Bromination of **4** at low temperature afforded 10,10'-dibromo-9,9'-bianthracene (**5**). **5** further reacted with (2,6-dimethylphenyl)boronic acid under Suzuki cross coupling conditions and provided 10-(2,6-dimethylphenyl)-9,9'-bianthracene (**6**) in a mixture of three byproducts, namely 9,9'-bianthracene (**6-1**), 10-bromo-9,9'-bianthracene (**6-2**) and 10,10'-bis(2,6-dimethylphenyl)-9,9'-bianthracene (**6-3**) (see Supporting Information). Owing to similar polarities of **6** and **6-1** to **6-3**, isolation of **6** by silica gel chromatography was hampered. Thus, the roughly purified compound mixture **6** was directly brominated at 0 °C, and **2** was obtained as a light-sensitive yellow solid with an overall yield of 5%. The purity of **2** was verified by nuclear magnetic resonance spectroscopy and high-resolution matrix-assisted laser desorption/ionization time-of-flight spectrometry.

Final edited form was published in "Journal of the American Chemical Society". 2019, 142 (3), S. 1147–1152. ISSN 1520-5126
https://doi.org/10.1021/jacs.9b09212


**Scheme 1. Synthetic route toward NGs 1a and 1b**[a,b]

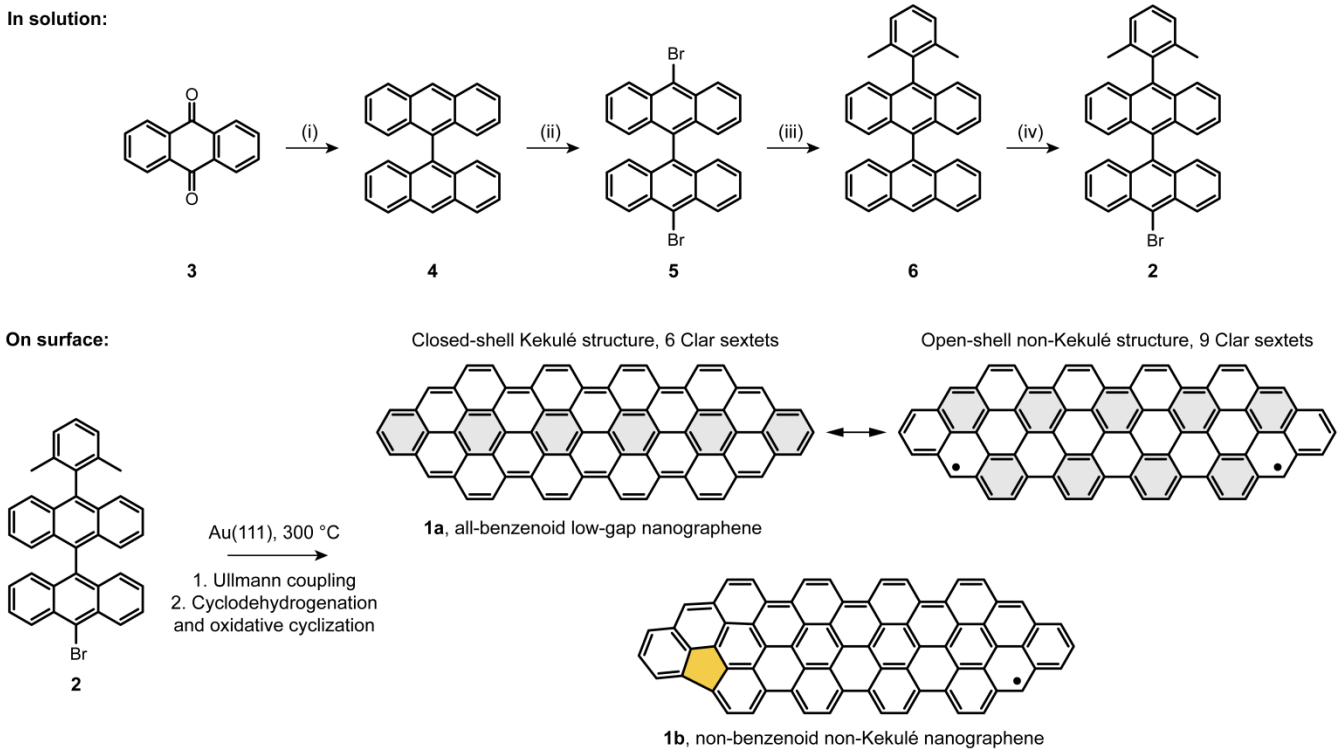


[a]Reagents and conditions: (i) Zn, $CH_3COOH$/HCl, 50 °C, overnight, 30%; (ii) $Br_2$, $CHCl_3$, 0 °C to room temperature, 2 h, 28%; (iii) 2,6-dimethylphenylboronic acid, $K_3PO_4$, DPEPhos, $Pd_2(dba)_3$, toluene/EtOH/$H_2O$, 110 °C, overnight; (iv) $Br_2$, $CHCl_3$, 0 °C to room temperature, overnight, 5%. [b]Gray filled rings denote Clar sextets.

Subsequently, a submonolayer coverage of **2** was deposited on a Au(111) surface held at room temperature, and annealed to 300 °C to promote on-surface reactions. Figure 1a presents an overview STM image of the surface, wherein individual molecules and covalently-bonded oligomers (Figure S1) are found. High-resolution (HR) STM imaging at low tunneling bias reveals that ~ 6% of the molecules (**1a**) exhibit a characteristic 2-lobed local density of states (LDOS) distribution at the termini (Figure 1b).

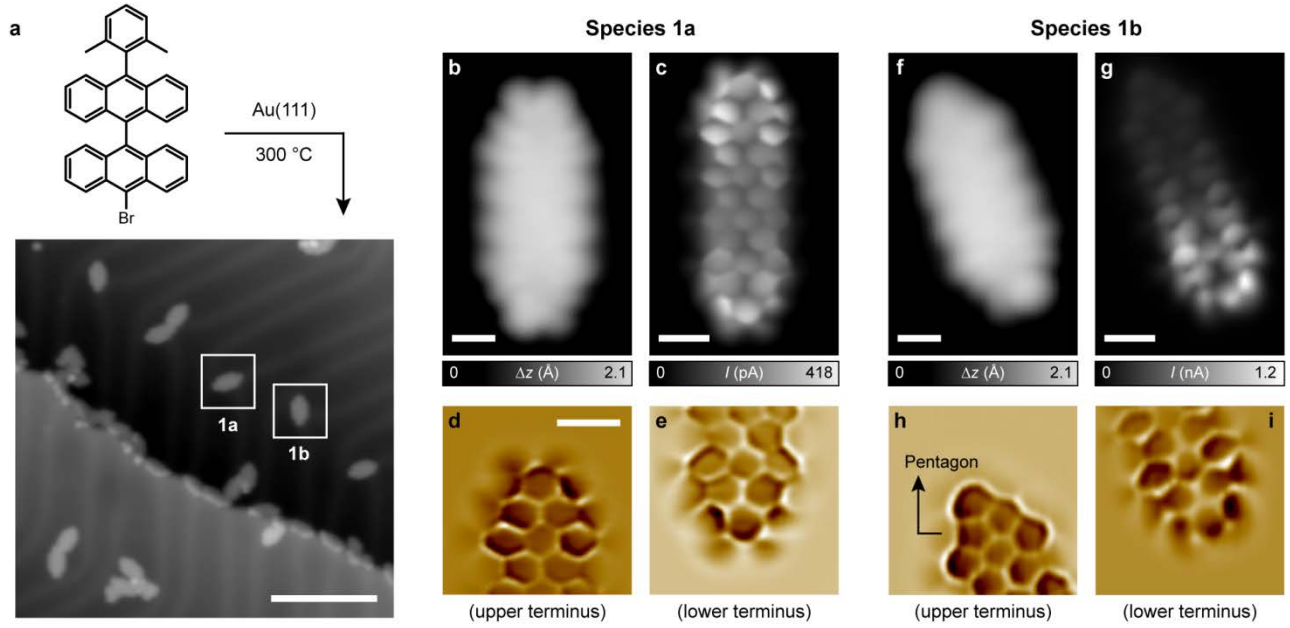


**Figure 1.** On-surface synthesis and structural characterization of **1a** and **1b**. (a) Overview STM topography image after annealing **2** on Au(111) at 300 °C. (b, c) HR-STM (b) and UHR-STM (c) images of **1a**. (d, e) Laplace-filtered UHR-STM images of the termini of **1a**. (f, g) HR-STM (f) and UHR-STM (g) images of **1b**. (h, i) Laplace-filtered UHR-STM images of the termini of **1b**. Scanning parameters: $V$ = -1 V, $I$ = 70 pA (a); $V$ = -100 mV, $I$ = 50 pA (b, f) and $V$ = -5 mV, $I$ = 50 pA, $\Delta z$ = -0.80 – -0.95 Å (c-e) and (g-i). Scale bars: 10 nm (a) and 0.5 nm (b-i). STM images in (b, f) are acquired with CO-functionalized tips.

Final edited form was published in "Journal of the American Chemical Society". 2019, 142 (3), S. 1147–1152. ISSN 1520-5126
https://doi.org/10.1021/jacs.9b09212

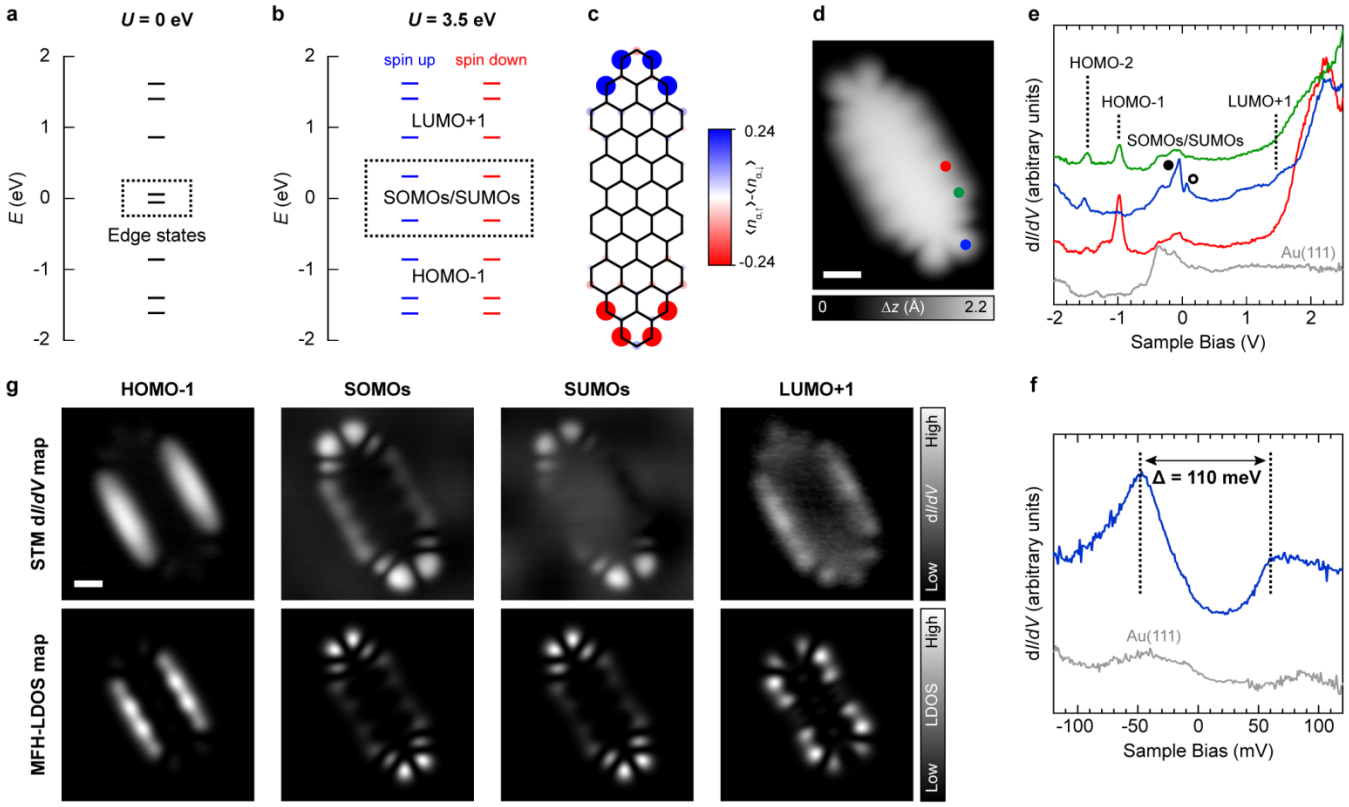


**Figure 2.** Electronic characterization of **1a**. (a, b) Nearest-neighbor TB (a) and MFH (b) energy spectrum of **1a**. (c) MFH spin density distribution of **1a**. Blue/red isosurfaces denote spin up/spin down density. (d) HR-STM image of **1a**. (e, f) d*I*/d*V* spectroscopy on **1a**. Acquisition positions are marked with corresponding filled circles in (d). The spectra in all panels are vertically offset for visual clarity. (g) Constant-current d*I*/d*V* maps (top panels) and simulated MFH-LDOS maps (bottom panels) of the HOMO-1, SOMOs, SUMOs and LUMO+1 of **1a**. Scanning parameters: $V$ = -30 mV, $I$ = 350 pA (d); $V$ = -980 mV, $I$ = 400 pA (g, HOMO-1); $V$ = -30 mV, $I$ = 350 pA (g, SOMOs); $V$ = +50 mV, $I$ = 400 pA (g, SUMOs) and $V$ = +1.45 V, $I$ = 400 pA (g, LUMO+1); $V_{rms}$ = 10 mV (g, SOMOs and SUMOs) and 22 mV (g, HOMO-1 and LUMO+1). Open feedback parameters for d*I*/d*V* spectra: $V$ = -2.00 V, $I$ = 370 pA (e) and $V$ = -50 mV, $I$ = 500 pA (f); $V_{rms}$ = 16 mV (e) and 2 mV (f). Scale bars: 0.5 nm.

We performed ultrahigh-resolution (UHR) STM imaging to gain access to the bond-resolved structure of the molecules.[35,36] Figures 1c-e present UHR-STM images of **1a**, confirming its all-benzenoid topology with the presence of triangulene-like termini, implying no loss of methyl groups from **2** during annealing. However, the majority of the molecules (~ 94%) exhibit different appearances at the two termini (**1b**). While one of the termini of **1b** presents a 2-lobed LDOS feature similar to **1a**, the other terminus exhibits a triangular topography with no discernible LDOS features at low tunneling bias (Figure 1f). Figure 1g presents the UHR-STM image of **1b**, revealing that at the lower terminus, the chemical structure is strongly convolved with LDOS near zero bias, in contrast to the upper terminus which does not exhibit any zero-bias LDOS. UHR-STM imaging of the termini shows the formation of a pentagonal ring at one of the termini (Figure 1h), with the other terminus retaining the triangulene-like structure (Figure 1i). Notably, the zero-bias LDOS accumulates almost exclusively on the triangulene-like terminus. Evidently, formation of a pentagonal ring implies the loss of a single methyl group from an Ullmann-coupled dimer of **2** (also see Figure S2).

To elucidate the electronic structures of the products, we employ the nearest-neighbor TB model. Figure 2a and Figure S3 present the TB energy spectrum of **1a**, which shows a pair of states located close to zero energy. These states are localized at the zigzag edges of the termini with a fast decay of wave function amplitude toward the center of the molecule, characteristic of edge states[37] (Figure S4). To account for electron-electron interactions in these localized states, we employ the MFH model, which leads to spin polarization in the system. The frontier electronic structure is characterized by a pair of singly occupied molecular orbitals (SOMOs, Figure 2b), with the populating spins aligned antiferromagnetically (Figure S5), in agreement with Ovchinnikov's rule[38] and previous ab-initio calculations.[39] The computed spin density distribution of **1a** (Figure 2c) reveals dominant spin localization at the zigzag carbon atoms at the termini, with spin up and spin down populations spatially separated. The experimental electronic structure of **1a** is characterized via STS, which reproduces the salient features of the TB/MFH calculations. As shown in Figure 2d,e, d*I*/d*V* spectroscopy on **1a** reveals a series of electronic resonances at -1.50 V (HOMO-2; HOMO is highest occupied molecular orbital), -980 mV (HOMO-1) and +1.45 V (LUMO+1; LUMO is lowest unoccupied molecular orbital), along with a broad peak at +2.23 V. Additionally, a pair of electronic resonances near zero bias are detected (Figure 2e, marked with filled and empty circles and labeled as SOMOs/SUMOs; SUMO is singly unoccupied molecular orbital). d*I*/d*V* spectroscopy in the vicinity of the Fermi level reveals two peaks at -50 mV and +60 mV (Figure 2f). Spatial mapping of the d*I*/d*V* signal (d*I*/d*V* maps) around -980 mV, -50 mV, +60 mV and +1.45 V (Figure 2g) exhibits excellent agreement with the mean-field Hubbard local density of states (MFH-LDOS) maps of the HOMO-1, SOMOs, SUMOs and LUMO+1 of **1a**, respectively. This confirms the spectroscopic features labeled in Figure 2e as molecular orbital resonances (also see Figures S6-S8). Based on the energies of the SOMOs and SUMOs, the frontier gap of **1a** is inferred to be 110 meV.

Final edited form was published in "Journal of the American Chemical Society". 2019, 142 (3), S. 1147–1152. ISSN 1520-5126
https://doi.org/10.1021/jacs.9b09212

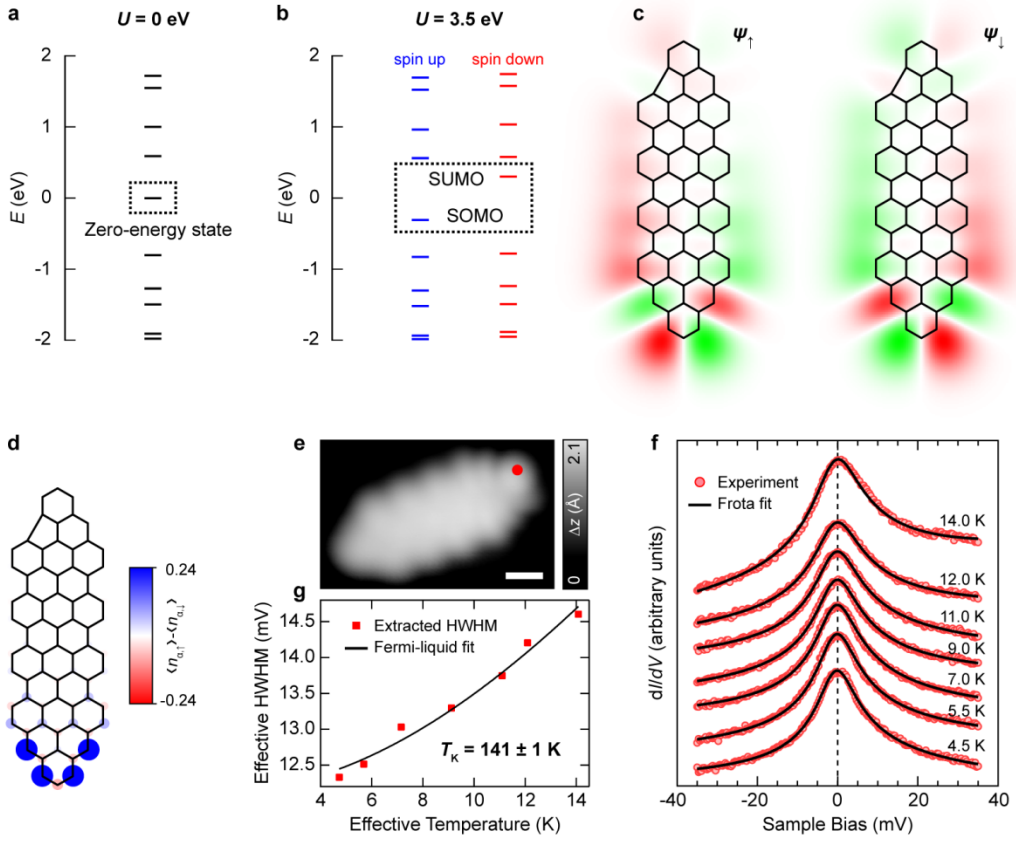


**Figure 3.** Electronic characterization of **1b**. (a, b) Nearest-neighbor TB (a) and MFH (b) energy spectrum of **1b**. (c) Computed wave functions of the SOMO ($\psi_\uparrow$) and SUMO ($\psi_\downarrow$) of **1b**. Green/red isosurfaces denote opposite phase of the wave function. (d) MFH spin density distribution of **1b**. (e) HR-STM image of **1b** (repeated from Figure 1f). (f) Temperature evolution of the Kondo resonance detected in **1b**, with corresponding fit using the Frota function.[40] Acquisition position is marked with a filled circle in (e). (g) Temperature evolution of the extracted half width at half maximum (HWHM) of the Kondo resonance, with fit using the Fermi-liquid model.[33] Open feedback parameters for d$I$/d$V$ spectra: $V$ = -35 mV, $I$ = 300 pA, $V_{rms}$ = 400 μV. Scale bars: 0.5 nm.

In contrast to the all-benzenoid topology of **1a**, the presence of a pentagonal ring in **1b** disrupts the bipartite symmetry of the underlying honeycomb lattice, and Ovchinnikov's rule cannot be applied to determine the ground state spin multiplicity. Importantly, presence of the pentagonal ring renders **1b** a non-Kekulé system, where no Kekulé valence structures can be drawn without leaving an unpaired electron (Scheme 1), making the system inherently magnetic with a spin $S$ = ½. Accordingly, the TB energy spectrum of **1b** (Figure 3a) reveals a zero-energy state occupied by one electron. Inclusion of on-site Coulomb repulsion triggers spin polarization, along with the opening of a Coulomb gap and a net spin imbalance of one in the system (Figure 3b). The computed spin-polarized wave functions of the SOMO and SUMO of **1b** is displayed in Figure 3c, which exhibit dominant localization at the zigzag edges of the triangulene-like terminus, with negligible amplitude at the pentagonal ring-containing terminus. The computed spin density distribution of **1b** (Figure 3d) reveals spin localization only at the triangulene-like terminus, in agreement with the spatial extent of the zero-bias LDOS (Figure 1g). The hallmark of a spin-½ system on a metal surface is screening of the individual spin by itinerant conduction electrons of the surface, leading to a many-body Kondo ground state.[33] d$I$/d$V$ spectroscopy on the triangulene-like terminus of **1b** reveals a pronounced zero-bias peak which exhibits an anomalous resonance linewidth broadening with increasing temperature, following the characteristic trend of a Kondo resonance with a Kondo temperature of $T_K$ ~ 141 K (Figure 3f,g; also see Figures S9 and S10). The detection of a Kondo resonance unambiguously establishes spin-½ paramagnetism in **1b**.

In summary, we have shown the synthesis of two open-shell NGs, **1a** and **1b**, resulting from the on-surface reactions of a single precursor **2** on Au(111). **1a** is an all-benzenoid NG containing a zigzag edge-rich terminus hosting low-energy edge states, with a frontier electronic gap of 110 meV. **1b** is a non-benzenoid NG with a single pentagonal ring in a benzenoid framework. Presence of this topological defect renders **1b** a non-Kekulé system with $S$ = ½, which is detected as a Kondo resonance. Our work demonstrates unambiguous experimental evidence of all-carbon magnetism, and provides rich opportunities to induce and tune magnetism in NGs through topological defects.

## ASSOCIATED CONTENT

### Supporting Information

The Supporting Information is available free of charge on the ACS Publications website.

Additional TB and MFH calculations, and STM/STS data (Figures S1-S10), detailed synthetic procedures of chemical compounds reported in this study (Schemes S1−S4), associated solution characterization data (Figures S11−S17), mathematical fit procedures for Kondo resonance, and experimental and calculation methods (PDF)

## AUTHOR INFORMATION

### Corresponding Author

*xinliang.feng@tu-dresden.de
*roman.fasel@empa.ch

### Notes

The authors declare no competing financial interests.

## ACKNOWLEDGMENT

This work was supported by the Swiss National Science Foundation (grant numbers 200020-182015 and IZLCZ2-170184), the European Union's Horizon 2020 research and innovation program under grant agreement numbers 696656 and 785219 (Graphene Flagship Core 2), the Office of Naval Research (grant number N00014-18-1-2708), ERC Consolidator grant (T2DCP, number 819698), the German Research Foundation (DFG) within the Cluster of Excellence – Center for Advancing Electronics Dresden (cfaed) and EnhanceNano (number 391979941), and the European Social Fund and the Federal State of Saxony (ESF-Project GRAPHD, TU Dresden).

## REFERENCES

(1) Yazyev, O. V. Emergence of Magnetism in Graphene Materials and Nanostructures. *Rep. Prog. Phys.* **2010**, *73* (5), 056501.

(2) Trauzettel, B.; Bulaev, D. V.; Loss, D.; Burkard, G. Spin Qubits in Graphene Quantum Dots. *Nat. Phys.* **2007**, *3* (3), 192–196.

(3) Yazyev, O. V.; Katsnelson, M. I. Magnetic Correlations at Graphene Edges: Basis for Novel Spintronics Devices. *Phys. Rev. Lett.* **2008**, *100* (4), 047209.

(4) Wang, W. L.; Yazyev, O. V.; Meng, S.; Kaxiras, E. Topological Frustration in Graphene Nanoflakes: Magnetic Order and Spin Logic Devices. *Phys. Rev. Lett.* **2009**, *102* (15), 157201.

(5) Bullard, Z.; Girão, E. C.; Owens, J. R.; Shelton, W. A.; Meunier, V. Improved All-Carbon Spintronic Device Design. *Sci. Rep.* **2015**, *5*, 7634.

(6) Narita, A.; Wang, X.-Y.; Feng, X.; Müllen, K. New Advances in Nanographene Chemistry. *Chem. Soc. Rev.* **2015**, *44* (18), 6616–6643.

(7) *On-Surface Synthesis*; Gourdon, A., Ed.; Springer International Publishing: Cham, 2016.

(8) Konishi, A.; Hirao, Y.; Nakano, M.; Shimizu, A.; Botek, E.; Champagne, B.; Shiomi, D.; Sato, K.; Takui, T.; Matsumoto, K.; Kurata, H.; Kubo, T. Synthesis and Characterization of Teranthene: A Singlet Biradical Polycyclic Aromatic Hydrocarbon Having Kekulé Structures. *J. Am. Chem. Soc.* **2010**, *132* (32), 11021–11023.

(9) Konishi, A.; Hirao, Y.; Matsumoto, K.; Kurata, H.; Kishi, R.; Shigeta, Y.; Nakano, M.; Tokunaga, K.; Kamada, K.; Kubo, T. Synthesis and Characterization of Quarteranthene: Elucidating the Characteristics of the Edge State of Graphene Nanoribbons at the Molecular Level. *J. Am. Chem. Soc.* **2013**, *135* (4), 1430–1437.

(10) Tönshoff, C.; Bettinger, H. F. Photogeneration of Octacene and Nonacene. *Angew. Chem. Int. Ed.* **2010**, *49* (24), 4125–4128.

(11) Krüger, J.; García, F.; Eisenhut, F.; Skidin, D.; Alonso, J. M.; Guitián, E.; Pérez, D.; Cuniberti, G.; Moresco, F.; Peña, D. Decacene: On-Surface Generation. *Angew. Chem. Int. Ed.* **2017**, *56* (39), 11945–11948.

(12) Zuzak, R.; Dorel, R.; Kolmer, M.; Szymonski, M.; Godlewski, S.; Echavarren, A. M. Higher Acenes by On-Surface Dehydrogenation: From Heptacene to Undecacene. *Angew. Chem. Int. Ed.* **2018**, *57* (33), 10500–10505.

(13) Urgel, J. I.; Mishra, S.; Hayashi, H.; Wilhelm, J.; Pignedoli, C. A.; Giovannantonio, M. D.; Widmer, R.; Yamashita, M.; Hieda, N.; Ruffieux, P.; Yamada, H.; Fasel, R. On-Surface Light-Induced Generation of Higher Acenes and Elucidation of Their Open-Shell Character. *Nat. Commun.* **2019**, *10* (1), 861.

(14) Ajayakumar, M. R.; Fu, Y.; Ma, J.; Hennersdorf, F.; Komber, H.; Weigand, J. J.; Alfonsov, A.; Popov, A. A.; Berger, R.; Liu, J.; Müllen, K.; Feng, X. Toward Full Zigzag-Edged Nanographenes: Peri-Tetracene and Its Corresponding Circumanthracene. *J. Am. Chem. Soc.* **2018**, *140* (20), 6240–6244.

(15) Mishra, S.; Lohr, T. G.; Pignedoli, C. A.; Liu, J.; Berger, R.; Urgel, J. I.; Müllen, K.; Feng, X.; Ruffieux, P.; Fasel, R. Tailoring Bond Topologies in Open-Shell Graphene Nanostructures. *ACS Nano* **2018**, *12* (12), 11917–11927.

(16) Rogers, C.; Chen, C.; Pedramrazi, Z.; Omrani, A. A.; Tsai, H.-Z.; Jung, H. S.; Lin, S.; Crommie, M. F.; Fischer, F. R. Closing the Nanographene Gap: Surface-Assisted Synthesis of Peripentacene from 6,6′-Bipentacene Precursors. *Angew. Chem. Int. Ed.* **2015**, *54* (50), 15143–15146.

(17) Li, Y.; Heng, W.-K.; Lee, B. S.; Aratani, N.; Zafra, J. L.; Bao, N.; Lee, R.; Sung, Y. M.; Sun, Z.; Huang, K.-W.; Webster, R. D.; Navarrete, J. T. L.; Kim, D.; Osuka, A.; Casado, J.; Ding, J.; Wu, J. Kinetically Blocked Stable Heptazethrene and Octazethrene: Closed-Shell or Open-Shell in the Ground State? *J. Am. Chem. Soc.* **2012**, *134* (36), 14913–14922.

(18) Zeng, W.; Gopalakrishna, T. Y.; Phan, H.; Tanaka, T.; Herng, T. S.; Ding, J.; Osuka, A.; Wu, J. Superoctazethrene: An Open-Shell Graphene-like Molecule Possessing Large Diradical Character but Still with Reasonable Stability. *J. Am. Chem. Soc.* **2018**, *140* (43), 14054–14058.

(19) Ruffieux, P.; Wang, S.; Yang, B.; Sánchez-Sánchez, C.; Liu, J.; Dienel, T.; Talirz, L.; Shinde, P.; Pignedoli, C. A.; Passerone, D.; Dumslaff, T.; Feng, X.; Müllen, K.; Fasel, R. On-Surface Synthesis of Graphene Nanoribbons with Zigzag Edge Topology. *Nature* **2016**, *531* (7595), 489–492.

(20) Li, J.; Sanz, S.; Corso, M.; Choi, D. J.; Peña, D.; Frederiksen, T.; Pascual, J. I. Single Spin Localization and Manipulation in Graphene Open-Shell Nanostructures. *Nat. Commun.* **2019**, *10* (1), 200.

(21) Morita, Y.; Suzuki, S.; Sato, K.; Takui, T. Synthetic Organic Spin Chemistry for Structurally Well-Defined Open-Shell Graphene Fragments. *Nat. Chem.* **2011**, *3* (3), 197–204.

(22) Goto, K.; Kubo, T.; Yamamoto, K.; Nakasuji, K.; Sato, K.; Shiomi, D.; Takui, T.; Kubota, M.; Kobayashi, T.; Yakusi, K.; Ouyang, J. A. A Stable Neutral Hydrocarbon Radical: Synthesis, Crystal Structure, and Physical Properties of 2,5,8-Tri-*tert*-butyl-phenalenyl. *J. Am. Chem. Soc.* **1999**, *121* (7), 1619–1620.

(23) Allinson, G.; Bushby, R. J.; Paillaud, J. L.; Oduwole, D.; Sales, K. ESR Spectrum of a Stable Triplet π Biradical: Trioxytriangulene. *J. Am. Chem. Soc.* **1993**, *115* (5), 2062–2064.

(24) Inoue, J.; Fukui, K.; Kubo, T.; Nakazawa, S.; Sato, K.; Shiomi, D.; Morita, Y.; Yamamoto, K.; Takui, T.; Nakasuji, K. The First Detection of a Clar's Hydrocarbon, 2,6,10-Tri-*tert*-Butyltriangulene: A Ground-State Triplet of Non-Kekulé Polynuclear Benzenoid Hydrocarbon. *J. Am. Chem. Soc.* **2001**, *123* (50), 12702–12703.

(25) Pavliček, N.; Mistry, A.; Majzik, Z.; Moll, N.; Meyer, G.; Fox, D. J.; Gross, L. Synthesis and Characterization of Triangulene. *Nat. Nanotechnol.* **2017**, *12* (4), 308–311.

(26) Mishra, S.; Beyer, D.; Eimre, K.; Liu, J.; Berger, R.; Gröning, O.; Pignedoli, C. A.; Müllen, K.; Fasel, R.; Feng, X.; Ruffieux, P. Synthesis

and Characterization of π-Extended Triangulene. *J. Am. Chem. Soc.* **2019**, *141* (27), 10621–10625.

(27) Su, J.; Telychko, M.; Hu, P.; Macam, G.; Mutombo, P.; Zhang, H.; Bao, Y.; Cheng, F.; Huang, Z.-Q.; Qiu, Z.; Tan, S. J. R.; Lin, H.; Jelínek, P.; Chuang, F.-C.; Wu, J.; Lu, J. Atomically Precise Bottom-up Synthesis of π-Extended [5]Triangulene. *Sci. Adv.* **2019**, *5* (7), eaav7717.

(28) Banhart, F.; Kotakoski, J.; Krasheninnikov, A. V. Structural Defects in Graphene. *ACS Nano* **2011**, *5* (1), 26–41.

(29) Cretu, O.; Krasheninnikov, A. V.; Rodríguez-Manzo, J. A.; Sun, L.; Nieminen, R. M.; Banhart, F. Migration and Localization of Metal Atoms on Strained Graphene. *Phys. Rev. Lett.* **2010**, *105* (19), 196102.

(30) Terrones, H.; Terrones, M.; Hernández, E.; Grobert, N.; Charlier, J.-C.; Ajayan, P. M. New Metallic Allotropes of Planar and Tubular Carbon. *Phys. Rev. Lett.* **2000**, *84* (8), 1716–1719.

(31) Lahiri, J.; Lin, Y.; Bozkurt, P.; Oleynik, I. I.; Batzill, M. An Extended Defect in Graphene as a Metallic Wire. *Nat. Nanotechnol.* **2010**, *5* (5), 326–329.

(32) Yazyev, O. V.; Louie, S. G. Electronic Transport in Polycrystalline Graphene. *Nat. Mater.* **2010**, *9* (10), 806–809.

(33) Ternes, M.; Heinrich, A. J.; Schneider, W.-D. Spectroscopic Manifestations of the Kondo Effect on Single Adatoms. *J. Phys. Condens. Matter* **2008**, *21* (5), 053001.

(34) Baumgarten, M.; Yüksel, T. Synthesis and Optical Properties of Novel Blue Fluorescent Conjugated Polymers. *Phys. Chem. Chem. Phys.* **1999**, *1* (8), 1699–1706.

(35) Gross, L.; Mohn, F.; Moll, N.; Liljeroth, P.; Meyer, G. The Chemical Structure of a Molecule Resolved by Atomic Force Microscopy. *Science* **2009**, *325* (5944), 1110–1114.

(36) Kichin, G.; Weiss, C.; Wagner, C.; Tautz, F. S.; Temirov, R. Single Molecule and Single Atom Sensors for Atomic Resolution Imaging of Chemically Complex Surfaces. *J. Am. Chem. Soc.* **2011**, *133* (42), 16847–16851.

(37) Pisani, L.; Chan, J. A.; Montanari, B.; Harrison, N. M. Electronic Structure and Magnetic Properties of Graphitic Ribbons. *Phys. Rev. B* **2007**, *75* (6), 064418.

(38) Ovchinnikov, A. A. Multiplicity of the Ground State of Large Alternant Organic Molecules with Conjugated Bonds. *Theor. Chim. Acta* **1978**, *47* (4), 297–304.

(39) Palma, C.-A.; Awasthi, M.; Hernandez, Y.; Feng, X.; Müllen, K.; Niehaus, T. A.; Barth, J. V. Sub-Nanometer Width Armchair Graphene Nanoribbon Energy Gap Atlas. *J. Phys. Chem. Lett.* **2015**, *6* (16), 3228–3235.

(40) Frota, H. O. Shape of the Kondo Resonance. *Phys. Rev. B* **1992**, *45* (3), 1096–1099.